Biochimica et Biophysica Acta 1798 (2010) 1961–1968

Contents lists available at ScienceDirect

Biochimica et Biophysica Acta

journal homepage: www.elsevier.com/locate/bbamem

The NMR solution structure of subunit G (G_{61-101}) of the eukaryotic V1VO ATPase from *Saccharomyces cerevisiae*

Sankaranarayanan Rishikesan, Malathy S.S. Manimekalai, Gerhard Grüber *

School of Biological Sciences, Nanyang Technological University, 60 Nanyang Drive, Singapore 637551, Republic of Singapore

ARTICLE INFO

Article history:
Received 27 April 2010
Received in revised form 14 June 2010
Accepted 15 June 2010
Available online 27 June 2010

Keywords:
Vacuolar-type ATPase
V_1V_O ATPase
Subunit G
Vma10p
Subunit *d*
Subunit E
Stalk subunit

ABSTRACT

Subunit G is an essential stalk subunit of the eukaryotic proton pump V_1V_O ATPase. Previously the structure of the N-terminal region, G_{1-59}, of the 13 kDa subunit G was solved at higher resolution. Here solution NMR was performed to determine the structure of the recombinant C-terminal region (G_{61-101}) of subunit G of the *Saccharomyces cerevisiae* V_1V_O ATPase. The protein forms an extended α-helix between residues 64 and 100, whereby the first five- and the last residues of G_{61-101} are flexible. The surface charge distribution of G_{61-101} reveals an amphiphilic character at the C-terminus due to positive and negative charge distribution at one side and a hydrophobic surface on the opposite side of the structure. The hydrophobic surface pattern is mainly formed by alanine residues. The alanine residues 72, 74 and 81 were exchanged by a single cysteine in the entire subunit G. Cysteines at positions 72 and 81 showed disulfide formation. In contrast, no crosslink could be formed for the mutant Ala74Cys. Together with the recently determined NMR solution structure of G_{1-59}, the presented solution structure of G_{61-101} enabled us to present a first structural model of the entire subunit G of the *S. cerevisiae* V_1V_O ATPase.

1. Introduction

The eukaryotic vacuolar-type H^+-ATPases (V_1V_O ATPase, V-ATPase) is described as nature's most versatile proton pump and is composed of a water-soluble V_1 and an integral membrane V_O subcomplex [1–4]. The V_1 sector is composed of eight subunits in a proposed stoichiometry of A_3:B_3:C_1:D_1:E_X:F_1:G_2:H_X [5]. The A and B subunits are arranged hexagonally and alternately around a central cavity in which a seventh mass is located [6,7]. The integral and proton transducting V_O domain contains six different subunits in a stoichiometry of a_1:d_1:c_{4-5}:c'_1:c''_1:e_1 [2]. The energy, needed for the proton translocation, is provided from the cleavage of ATP into ADP and inorganic phosphate, catalyzed in the A_3:B_3 hexamer of the V_1 headpiece. Under certain physiological conditions both domains can undergo a reversible disassembly, a phenomenon unique for eukaryotic vacuolar H^+-ATPases [8–10]. A comparison of independently identified V_1 structures reveals that a compact stalk protrudes from the bottom of the A_3:B_3 hexamer with a length of 11 nm [6,11,12]. The stalk subunits undergo rearrangements when the V_1 ATPase reassembles with the V_O sector to form the entire V_1V_O complex as shown by crosslinking experiments, in which H-E, H-F crosslinks are observed in the V_1 sector and C-E crosslink in the V_1V_O ATPase [13,14], by electron microscopy images [15]. Since the assembled V_1V_O ATPase and the dissociated V_1 sector as well as the coupling process are of physiological relevance, the structure and topology of these stalk subunits are of great interest. Insight into the structural traits of stalk subunits came from the low resolution- [16] and crystallographic structure of subunit C [17], and H [18]. Subunit C has an elongated boot-shaped feature [16] with an upper head domain, a large globular foot and an elongated neck domain [17]. Stalk subunit H is characterized by a large, primarily α-helical N-terminal domain, forming a shallow groove, and a C-terminal domain, both connected by a four-residue loop [18]. Subunit G of the V-ATPase from yeast in solution was shown to be elongated [19]. Amino acid sequence alignments of G subunits from different species and of variable subunit G isoforms are highly conserved, whereas their carboxyl-terminal regions are variable [20–23]. The NMR solution structure of the N-terminal region, G_{1-59}, of the V-ATPase from *Saccharomyces cerevisiae* was described recently, showing an extended α-helix between residues 10 and 56, whereby the first nine and the last three residues of G_{1-59} are flexible [24].

Here, we have turned our focus to the production and purification of residues 61 to 101 of subunit G (G_{61-101}) from *S. cerevisiae* V_1V_O ATPase, which forms the remaining unsolved structural segment of subunit G. The structural features of the recombinant G_{61-101} were determined in solution using NMR spectroscopy. The introduction of a single cysteine residue into entire *S. cerevisiae* subunit G at three positions, forming three mutant proteins, resulted in different intersubunit disulfide patterns, which give insight into the proximity of the residues.

* Corresponding author. Tel.: +65 6316 2989; fax: +65 6791 3856.
E-mail address: ggrueber@ntu.edu.sg (G. Grüber).

0005-2736/$ – see front matter © 2010 Elsevier B.V. All rights reserved.
doi:10.1016/j.bbamem.2010.06.012

2. Materials and methods

2.1. Biochemicals

ProofStart™ DNA Polymerase and Ni^{2+}-NTA-chromatography resin were received from Qiagen (Hilden, Germany); restriction enzymes were purchased from Fermentas (St. Leon-Rot, Germany). Chemicals for gel electrophoresis were received from Serva (Heidelberg, Germany). Bovine serum albumin was purchased from GERBU Biochemicals (Heidelberg, Germany). ($^{15}NH_4$)Cl and (^{13}C) glucose were purchased from Cambridge Isotope Laboratories (Andover, USA). All other chemicals were at least of analytical grade and received from BIOMOL (Hamburg, Germany), Merck (Darmstadt, Germany), Roth (Karlsruhe, Germany), Sigma (Deisenhofen, Germany), or Serva (Heidelberg, Germany).

2.2. Expression and purification of the proteins

G_{61-101} was cloned from *S. cerevisiae* genome through PCR cloning method using 5'ATG GAT AAT GCC GGT GGT GTT G 3' as forward primer and 5' CGT TCG AGC TCC TAA GTC TCG ATC AAG ATC T 3' as reverse primer. PCR products incorporating *Nco*I and *Sac*I restriction sites were digested and ligated to pET9d(+)-His_3 vector [25]. To express the protein, liquid culture was shaken in LB medium containing kanamycin (30 mg ml^{-1}) for about 6 h at 37 °C until an optical density OD_{600} of 0.6–0.7 was reached. The uniform ^{15}N- and $^{15}N/^{13}C$-labeled G61–101 was expressed in *Escherichia coli* BL21 (DE3) cells using M9 minimal media containing $^{15}NH_4Cl$, or $^{15}NH_4Cl$ plus [U-^{13}C]-glucose. To induce production of proteins, cultures were supplemented with isopropyl-β-D-thio-galactoside (IPTG) to a final concentration of 1 mM. Following incubation for another 4 h at 30 °C, the cells were harvested at 8000*g* for 15 min at 4 °C. Subsequently, all cells were lysed on ice by sonication for 3 × 1 min at 50% power in the buffer (50 mM HEPES, pH 7.5, 200 mM NaCl, 1 mM DTT and 1 mM PMSF). The lysate was cleared by centrifugation at 10,000*g* for 30 min at 4 °C, the supernatant was passed through a filter (0.45 mm pore-size) and supplemented with Ni^{2+}-NTA resin. The His-tagged protein was allowed to bind to the matrix for 2 h at 4 °C by mixing on a sample rotator (Neolab), and eluted with an imidazole-gradient (25–250 mM) in the buffer. Fractions containing His-tagged proteins were identified by SDS-PAGE [26], pooled and concentrated using Centriprep YM-3 (3 kDa molecular mass cut-off) spin concentrators (Millipore) and subsequently applied on a gel filtration column Superdex HR75 (10/30, Amersham Biosciences), equilibrated with buffer composed of 50 mM HEPES (pH 7.5) 200 mM NaCl, 1 mM DTT, 1 mM PMSF and 5 mM ethylenediaminetetraacetic acid (EDTA). Selected fractions were concentrated in 3 kDa cut-off centricon. The purity of the protein sample was analysed by SDS-PAGE [26]. The SDS-gels were stained with Coomassie Brilliant Blue R250. Protein concentrations were determined by the bicinchoninic acid assay (BCA; Pierce, Rockford, IL, USA).

The single mutants A72C, A74C and A81C of the entire subunit G were generated by overlap extension polymerase chain reaction (PCR) method using the *Vma10* gene as a template. In two PCR reactions mutations were introduced by internal primers: Ala72Cys internal forward, 5′-GAA TTG GAA AAG AAA TGT GAG GCT GGT GTG-C-3′; Ala72Cys internal reverse 5′-GCA CAC CAG CCT CAC ATT TCT TTT CCA ATT C-3′; Ala74Cys internal forward 5′-GAA AAG AAA GCA GAG TGT GGT GTG CAA GGT GAA-3′; Ala74Cys internal reverse 5′- TTC ACC TTG CAC ACC ACA CTC TGC TTT CTT TTC-3′; Ala81Cys internal forward 5′- GTG CAA GGT GAA TTA TGC GAG ATT AAG AAA ATT GC-3′; Ala81Cys internal reverse 5′-GCA ATT TTC TTA ATC TCG CAT AAT TCA CCT TGC AC-3′. Mutated gene constructs of subunit G were finally amplified using flanking primers 5′-TTT CCA TGG CCT CCG CTA TTA CTG-3′ (forward primer *a*) and 5′-CGT TCG AGC TCT TAG CAC AAG GCA TTG ATA TG-3′ (reverse primer *d*). Following digestion with *Nco*I and *Sac*I restriction enzymes, the PCR products were ligated into the pET9d-His3 vector [26]. The mutations were verified by DNA sequencing. The protein production of these mutants was done as described above.

2.3. CD spectroscopy of G_{61-101}

Steady state CD spectra of G_{61-101} were measured in the far UV-light (190–260 nm) using a CHIRASCAN spectrometer (Applied Photophysics). Spectra were collected in a 60 µl quartz cell (Hellma) at 20 °C at a step resolution of 1 nm. The readings were average of 2 sec at each wavelength and the recorded milli-degree values were the average of three determinations for the sample. The CD spectrum was acquired in a buffer of 25 mM phosphate (pH 6.8), 200 mM NaCl and 5 mM EDTA with a protein concentration of 2.0 mg/ml. The spectrum for the buffer was subtracted from the spectrum of G_{61-101}. CD values were converted to mean residue molar ellipticity (θ) in units of $deg \times cm^2 \times dmol^{-1} \times aa^{-1}$ using the software *Chirascan Version 1.2*, Applied Photophysics. This baseline corrected spectrum was used as input for computer methods to obtain predictions of secondary structure.

2.4. NMR data collection and processing

The NMR sample, G_{61-101} was prepared in 90% H_2O / 10% D_2O containing 25 mM NaH_2PO_4 (pH 6.8), 200 mM NaCl, 5 mM EDTA and 0.1% NaN_3. All NMR experiments were performed at 303 K on a Bruker Avance 600 MHz spectrometer. The spectra recorded on $^{15}N/^{13}C$-labelled sample were HNCO, CBCA(CO)NH, HNCACB and 3D ^{15}N-NOESY-HSQC. The 3D ^{15}N-NOESY-HSQC was recorded using mixing time of 200 ms. All the two- and three-dimensional experiments made use of pulsed-field gradients for coherence selection and artifact suppression, and utilized gradient sensitivity enhancement schemes. Quadrature detection in the indirectly detected dimensions was achieved using either the States/TPPI (time-proportional phase incrementation) or the echo/anti-echo method. Baseline corrections were applied wherever necessary. The proton chemical shift was referenced to the methyl signal of DSS (2, 2-dimethyl-2-silapentane-5-sulphonate; Cambridge Isotope Laboratories) as an external reference to 0 ppm. The ^{13}C and ^{15}N chemical shifts were referenced indirectly to DSS. All the NMR data were processed using Bruker Avance spectrometer in-built software Topspin2.1 version. Peak-picking and data analysis of the Fourier transformed spectra were performed with the SPARKY program [27].

2.5. NMR spectroscopy and structure calculation of G_{61-101}

The additional His-residues of the His-tag at the N-terminus of G_{61-101}, which are essentially unstructured, were not used in the structure calculation. The structure calculation was performed from

Fig. 1. SDS gel (17% total acrylamide and 0.4% crosslinked acrylamide) of the recombinant G_{61-101} of the *S. cerevisiae* V-ATPase.

the first methionine in the N-terminal which is after the proline residue. The sequential assignments were achieved using triple-resonance backbone experiments (HNCO, HNCACB and CBCA(CO)NH) and all the side chain assignments were done using (H)CCCONH experiment. Dihedral angle restraints were calculated from C^{α} and C^{β} chemical shifts by using PREDITOR [28]. Distance constraints collection and structure reconstruction were performed on CYANA 3.0 package [29,30] using the manually picked NOE's from ^{1}H–^{15}N NOESY-HSQC on SPARKY software [27] and leading to 613 meaningful NOE distance restraints. 10 conformers of the monomeric G_{61-101} were calculated based on the obtained dihedral angles and NOE restraints. The program MOLMOL was used to visualize the ensemble of minimized conformers [31]. The coordinates for the structure of G_{61-101} were deposited in the Protein Data Bank with code 2KWY.

2.6. Diffusion coefficient measurement

The translational diffusion rates were measured by monitoring 1D ^{1}H signal decay due to molecular diffusion in the z-direction of the sample using PFGs [32,33] at variable concentrations of G_{61-101}. In each experiment the PFG strength was linearly incremented from 2 to 95 G/cm, with a translational diffusion delay of 200 ms and total

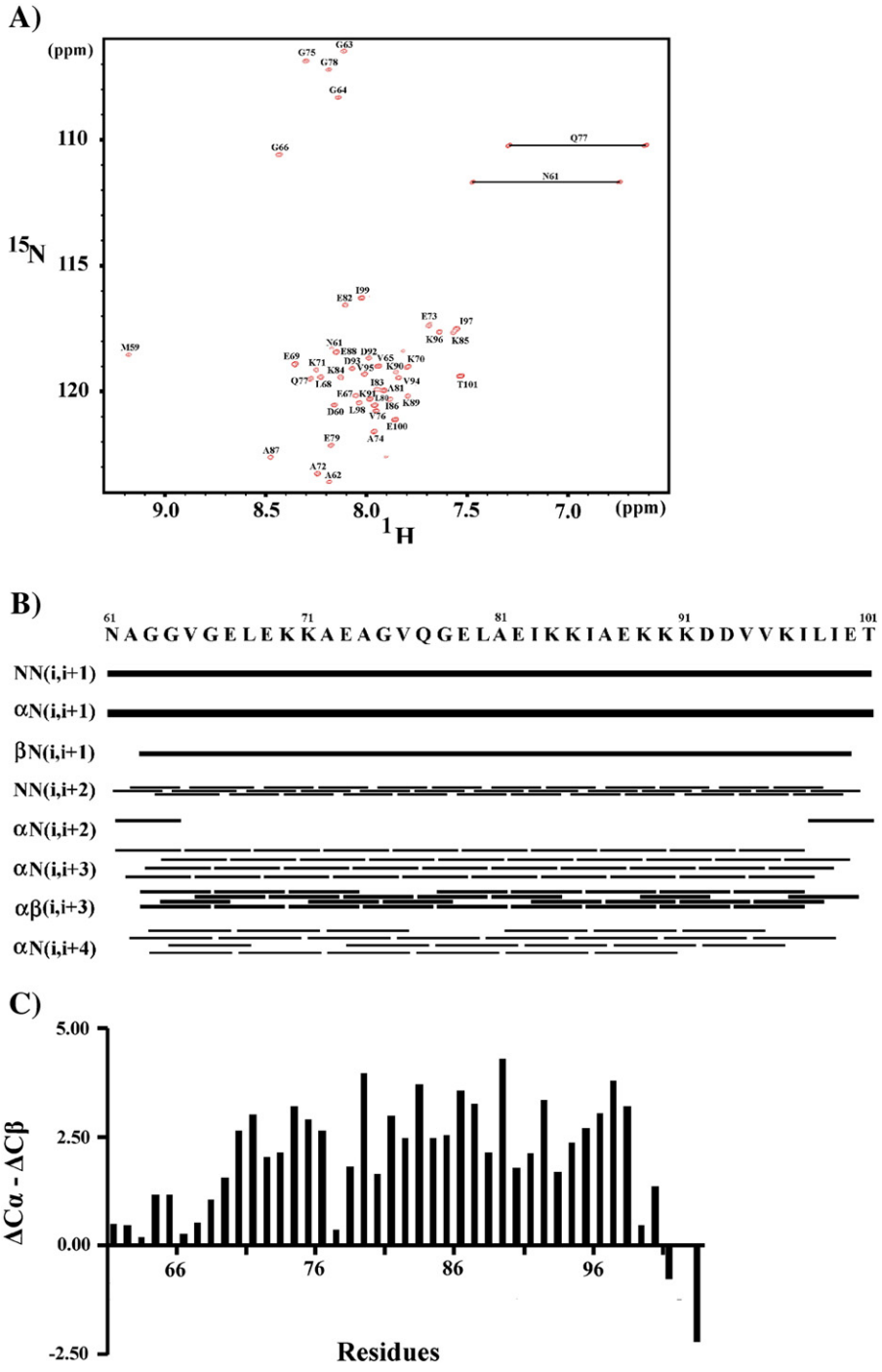

Fig. 2. (A) 2D ^{1}H–^{15}N-HSQC spectrum of *S. cerevisiae* G_{61-101} in 25 mM sodium phosphate buffer (6.8), 200 mM NaCl and 5 mM EDTA at 303 K. Signals from the side-chain NH_2 groups are connected by horizontal lines. (B) The NOESY connectivity plot of G_{61-101} indicative of the residues connected in space revealing the presence of helical structure. (C) Secondary chemical shifts ($\Delta^{13}C\alpha$–$\Delta^{13}C\beta$) of G_{61-101} in 25 mM sodium phosphate buffer (6.8), 200 mM NaCl and 5 mM EDTA at 303 K.

encoding and decoding gradient durations of 5 ms. The diffusion rates were estimated using TopSpin (Bruker BioSpin).

2.7. Cross-link formation of the cysteine mutants

The G subunit mutants Ala72Cys, Ala74Cys and Ala81Cys, respectively, were supplemented with 5 μM of $CuCl_2$ as a zero length cross-linker for 20 min on a sample rotator at 4 °C. The reaction was stopped by addition of 1 mM ethylenediaminetetraacetic (EDTA). Samples were dissolved in DTT-free dissociation buffer, and applied to an SDS-polyacrylamide gel as described above.

2.8. Dimer model of G_{61-101}

The average model of the NMR structure of G_{61-101} was docked with itself in order to identify the dimer formation. Docking studies were performed using the web interface of the protein docking software GRAMM [34], which does a global search using the Fast Fourier Transform methodology to identify the best rigid body conformations between the two proteins. The first fifty complex configurations were analyzed, which were scored based on soft Lennard–Jones potential, evolutionary conservation of predicted interface, statistical residue–residue preference, volume of the minimum, empirical binding free energy and atomic contact energy. The best docking model was chosen from this 50 complex configurations in such a way that it should have not more than 8 Å distance for the Cα atoms of the Ala72 and Ala81 with Ala72' and Ala81', respectively, in the dimer complex. This dimer model was then optimized using the program Swiss-PdbViewer 3.7 [35] by carrying out energy minimization *in vacuo* with the GROMOS96 43B1 parameter set, without reaction field as implemented in the program. For fast energy convergence initially 200 steps of Steepest Descent protocol was carried out followed by multiple steps of Conjugate Gradient technique until the derivative convergences to 0.050 kJ/mol.

3. Results

3.1. Protein production and purification of G_{61-101}

The SDS-PAGE of the recombinant *S. cerevisiae* G_{61-101} revealed a prominent band at about 4.5 kDa, which was found entirely within the soluble fractions. A Ni^{2+}-NTA resin column and an imidazole-gradient (25–250 mM) in 50 mM HEPES, pH 7.5, 200 mM NaCl, 1 mM DTT and 1 mM PMSF was used to purify the protein. The elution fractions from the Ni^{2+}-NTA purification containing the G_{61-101} were collected and were subsequently applied on to a gel filtration column Superdex HR75 (10/30, Amersham Biosciences). Analysis of the isolated protein by SDS-PAGE revealed the high purity of G_{61-101} (Fig. 1A). The secondary structure of G_{61-101} was determined from circular dichroism spectra that were measured between 190 and 260 nm (Supplementary Fig. S1). The minima at 222 and 208 nm and the maximum at 192 nm indicate the presence of α-helical structures in the protein. The average secondary structure content was 73% α-helix and 27% random coil.

3.2. Resonance assignment of G_{61-101}

Assignment for the backbone HN, N, Cα, Cβ, and C' resonance of the G_{61-101} was achieved by a combined analysis of the triple resonance HNCACB, CBCA(CO)NH and HNCO spectra. Fig. 2A shows the good quality of the assigned HSQC spectrum indicating backbone HN and ^{15}N cross peaks of all the residues of G_{61-101}. Overall, the limited chemical shift dispersion of around ~2.0 ppm for the amide proton resonances (Fig. 2B) may indicate predominantly helical proteins [36].

3.3. NMR derived 3-dimensional structure of *S. cerevisiae* G_{61-101}

Two- and three dimensional NMR experiments were performed to observe the solution structure of this protein. The structure of G_{61-101} was calculated on the basis of a total 613 non-trivial NMR-derived distance restraints. Hydrogen bonds were identified from the characteristic patterns of homonuclear ^1H nuclear Overhausser enhancements (NOEs) [36] and were introduced at the end of structure calculations. Typical α-helical NOE pattern $d_{\alpha N}(i,i+3)$, $d_{\alpha N}(i,i+4)$ and $d_{\alpha\beta}(i,i+3)$ were observed from the amino acid residues 64 to 100 (Fig. 2B). Secondary structure prediction was done by using the HA chemical shifts, which shows that G_{61-101} is mainly folded as an α-helical structure (Fig. 2C). Fig. 3A shows the overlay of the 10 lowest energy structures of G_{61-101} and the structural statistics are given in Table 1. These structures have an overall RMSD of 0.32 Å for the backbone atoms and 1.72 Å for all the heavy atoms in the helical region of the three

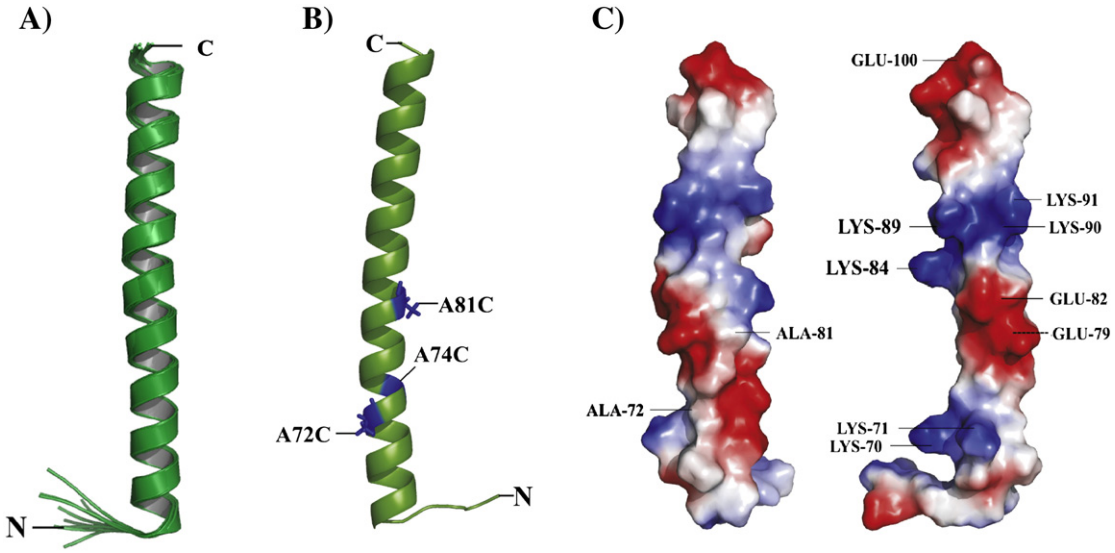

Fig. 3. Ribbon diagram of the NMR solution structure of *S. cerevisiae* G_{61-101}. (A) Best fit superimposition of the 10 lowest-energy NMR structures. Side view of the average structure of G_{61-101} (B), illustrating the relative positions of alanine residues 72, 74 and 81 inside the α-helix, which are marked in blue color. (C) Different orientations of G_{61-101}, showing the molecular surface with the electrostatic potential of the peptide, drawn in PyMol [47] that uses Poisson–Boltzmann equation, where the positive potentials are drawn in blue and negative in red color.

Table 1
Structural statistics for the 10 selected structures of G_{61-101} of the *S. cerevisiae* V-ATPase.

Total number of NMR restraints	613
Number of unambiguous NOE peaks	
Intraresidual ($\|i–j\|=0$)	192
Sequential ($\|i–j\|=1$)	201
Medium-range ($2\leq\|i–j\|\leq5$)	108
Long-range ($\|i–j\|>5$)	0
Number of dihedral angle constraints	77
Number of hydrogen-bond distance restraints	35
Number of restraint violations	
Total number of restraint violations >0.3 Å	0
Total number of dihedral angle violations >5°	0
Ramachandran plot statistics (%)	
Fractions of residues of most favoured regions (%)	94.7
Fractions of residues in additionally allowed regions (%)	5.3
Fractions of residues in generously allowed regions (%)	0
Fractions of residues in disallowed regions (%)	0
Structural precision of well-ordered region	
RMSD backbone (residues (64–100)	0.32 Å
RMSD heavy (residues 64–100)	1.72 Å

dimensional structures (residues 64–100) of the protein. All these structures have energies lower than 4 kcal/mol, no NOE violations greater than 0.3 Å, and no dihedral violations greater than 5 Å. The protein has an extended helical structure from the residues Gly64 to Glu100 measuring a length of 47.93 Å excluding the unstructured region in the N- (residues 59–63) and C-terminal ends (amino acid 101), as predicted from the amino acid sequence and the secondary structure prediction from the C-terminus of subunit G.

3.4. Translational diffusion rates of G_{61-101}

Subunit G of the *S. cerevisiae* V-ATPase is dimeric in solution as shown from solution X-ray scattering data [19]. As described recently, dimerization and oligomerization are important for the structure and functionality of soluble as well as membrane bound peptides or proteins [37,38]. Therefore, we analyzed the dimeric feature of G_{61-101} by measuring the diffusion coefficients of the protein as a function of protein concentration. The decrease in the experimentally determined diffusion rates with the increasing concentration of G_{61-101} suggested a dimer formation (Fig. 4), assuming that the exchange rate between monomer and dimer is fast on the diffusion timescale. The corresponding dimer dissociation constant for G_{61-101} was estimated by direct fit of the translation diffusion rates as a function of concentration to be 1.5 mM.

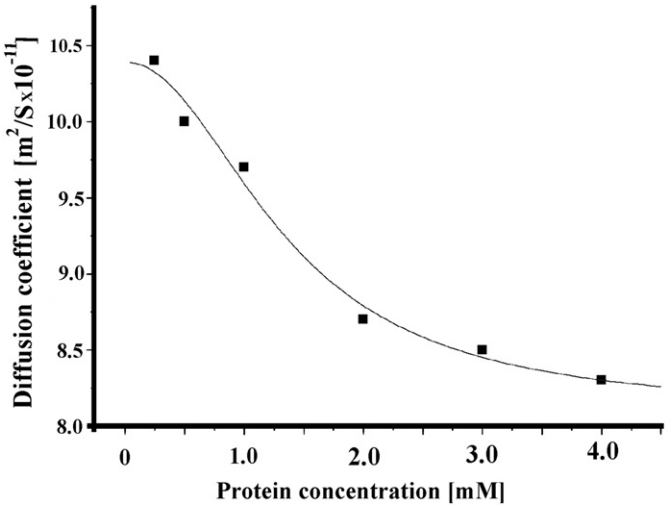

Fig. 4. Plot showing the change of diffusion coefficient versus concentration for G_{61-101}.

3.5. Crosslink formation of cysteine mutants of G subunit

The solution structure of G_{61-101} showed a strip of hydrophobic alanine residues like Ala72, Ala74 and Ala81 with a twist to each other (Fig. 3C). To analyze the proximity of the alanine residue of the first and second α helix of the dimeric G_{61-101}, Ala72, Ala74 and Ala81, respectively, were replaced by a cysteine residue, generating soluble and mono-disperse mutant proteins of entire subunit G. All three mutant proteins were isolated in high amounts and in high purity (Fig. 5A). Cross-linking formation in the presence of $CuCl_2$ (5 μM) is shown in Fig. 5B (lanes 1 and 3) for G_{61-101}, revealing that a significant amount of dimer formation could be generated for the two mutants Ala72 and Ala81. In contrast, when the alanine residue 74, located opposite to Ala72 on G_{61-101} (Fig. 3B) in the helix, was exchanged by a cysteine, no significant disulfide bond formation could be detected under the conditions used (Fig. 5B, lane 2).

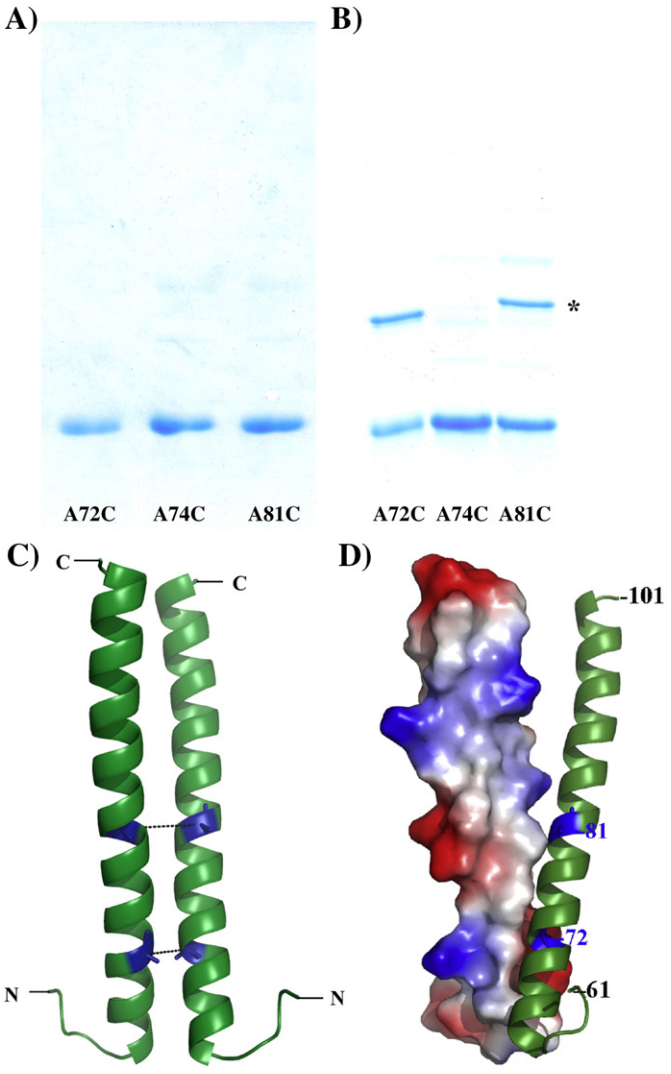

Fig. 5. SDS polyacrylamide gel (17% total acrylamide and 0.4% crosslinked acrylamide) of the (A) produced and purified subunit G mutants Ala72Cys, Ala74Cys and Ala81Cys and (B) Cross-linking of entire subunit G mutants Ala72Cys, Ala74Cys and Ala81Cys, respectively, in the presence of 5 μl of $CuCl_2$. (C) Dimeric model of G_{61-101} based on cross linking and docking data. Residues in blue color exhibiting Ala74 and Ala81 which form a zero-length crosslink in the subunit G mutants Ala72Cys and Ala81Cys when $CuCl_2$ is present. (D) The dimeric model showing the interaction through the hydrophobic patch. The molecular surface with the electrostatic potential is shown for one of the monomer (positive potentials are drawn in blue and negative in red color) and the residues Ala72 and Ala81 are shown in blue colour in the other monomer.

3.6. Dimerization interactions in G_{61-101}

The average model from the solution NMR structure of G_{61-101} was docked with itself to determine the dimer model (see Materials and methods). The best docking model chosen had less than 8 Å distance on the respective alanine positions at 72, 72' and 81, 81' in the dimeric complex (Fig. 5C). The docking energy for this model was calculated to be −175.26 kJ/mol using the formula, Docking energy = Energy of the dimer −2 * Energy of the subunit G_{61-101}; where the final minimized energies of the dimer and subunit G_{61-101} are −1627.20 and −725.97 kJ/mol, respectively. In the dimer model the NMR solution structures of G_{61-101} are arranged in a parallel orientation. The helical monomers are tilted by an angle of 21.5° with respect each other so as to interact through the hydrophobic patch along the helices (Fig. 5D). Comparatively the N-terminal regions of the monomers, where the hydrophobic patch is located, is close to each other which then deviates apart as it moves towards the C-terminal during dimer formation. Specifically Val65, Leu68, Ala72, Val76 and Leu80 have hydrophobic interactions with their dimeric partners Val65', Leu68', Ala72', Val76' and Leu80', respectively. The buried surface due to the dimer formation is calculated to be 618.2 $Å^2$ which represents 15% of the structure being buried inside. More specifically Leu68, Val76 and Leu80 show maximum buried surface area due to dimer formation. Further the solvation energy gained due to the complex formation is calculated to be −6.8 kcal/mol.

4. Discussion

The recently determined NMR solution structure of the recombinant 59 residues long N-terminus of the yeast V-ATPase subunit G yields an extended α-helical structure from the residues Thr_{10} to Ala_{56} with a length of 67.9 Å [24]. The surface charge distribution on one side of G_{1-59} showed a strip of negative amino acids at the C-terminus, whereby its N-terminus has a more amphiphilic character due to positive and negative charge distribution, attributed by the residues Lys5, Lys16, Lys24, Arg26 and Lys27 and Glu15, Glu17, Glu20, respectively. On the opposite side the structure of G_{1-59} revealed a hydrophobic surface at the N-terminus, made-up by the residues Val2, Ile8, Ala9, Leu11, Ala14, Ala18, Ala25 and Val22. NMR-titration experiments of G_{1-59} demonstrated that subunit G assembles with subunit *d* and that this binding occurs via the more hydrophobic epitope at the very N-terminus, characterized by the hydrophobic residues as well as with a charged segment, formed by the amino acids Lys16, Glu15, Glu17, Glu20, Lys24, Arg26, Lys27 and Asp31 [24]. These data confirmed the results, derived from amino acid substitution of subunit G residues Glu15 to Ala and deletions of Val22 and Asp31, respectively, which exhibited loss in ATPase activity [21]. The structure of G_{1-59} showed that these residues form a strip and therefore, substitution or deletion of one of these residues might cause a weaker interaction of both subunits G and *d*. By comparison, no binding could be detected, when the ^{15}N labeled recombinant G_{61-114} was titrated with subunit *d*, indicating that the subunit *d* binds only via the N-terminal segment of subunit G [24]. In parallel, NMR- and fluorescence correlation spectroscopy results also showed that the subunits E and G associate with each other [39] and moreover, excluded, together with the biochemical data published by Jones et al. [40] that subunits E and G form a coiled-coiled interaction over the length of both molecules as proposed recently [41]. In addition, the first 18 N-terminal residues of subunit E interact with one subunit C [40], whereas the 78 amino acid domain of E is required for assembly with subunit H [42]. These phenomena indicate that the two or three copies of G and E subunits, respectively [43], have different binding partners in their N-terminal parts, implying different roles inside the V_1V_O complex [5].

Solution X-ray scattering data revealed that subunit G is elongated and dimeric in solution [19], with an α-helical and highly conserved N-terminal half, and a proposed α-helical C-terminal sequence [21,44]. The presented NMR solution structure of G_{61-101} leads to a more complete understanding of the structural puzzle of stalk subunit G, and gives insight about a segment which was the least defined in subunit G. The C-terminal segment of subunit G from yeast V-ATPase is highly charged and predicted to interact with the subunits A and B [12,14]. The surface charge distribution of G_{61-101} shows a high degree of negative amino acids at one side and hydrophobic amino acids on

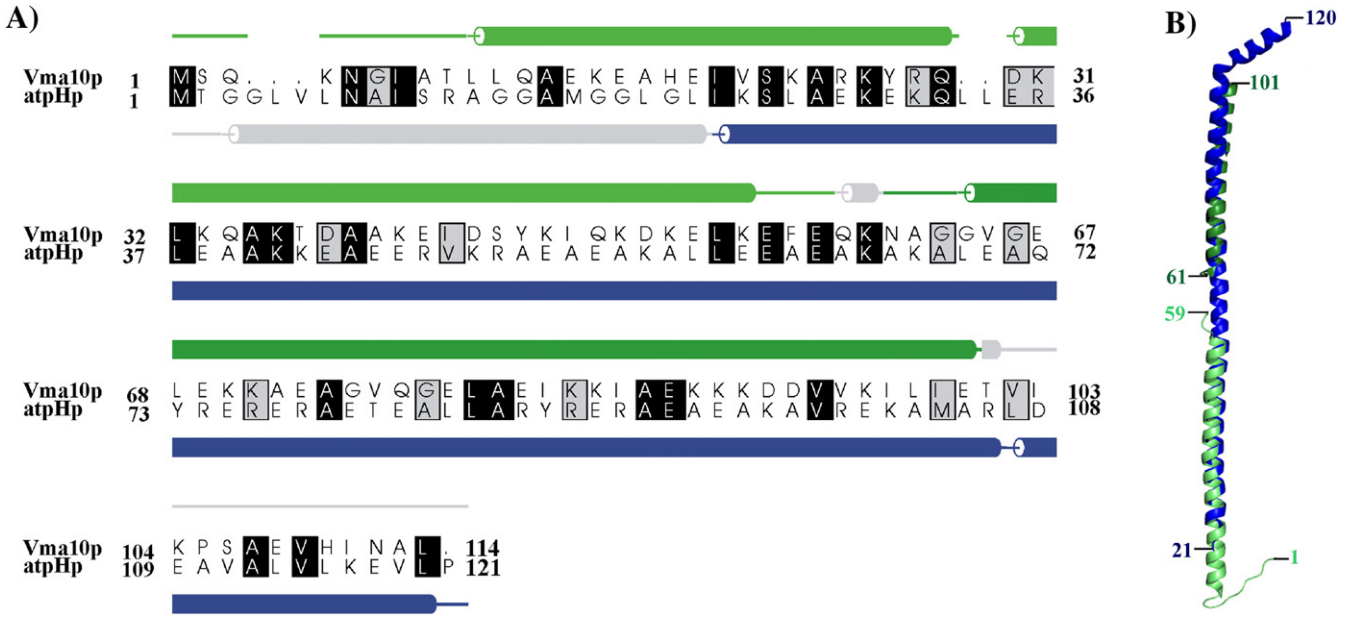

Fig. 6. Amino acid sequence of V-ATPase subunit G from *Saccharomyces cerevisiae* and subunit H of the *Thermus thermophilus* A_1A_O ATP synthase. The identical and homologue amino acid residues conserved between both the proteins are highlighted in black and grey color, respectively. The secondary structures based on the crystallographic models of subunit H of the *T. thermophilus* A_1A_O ATP synthase (blue, PDB code 3K5B [44]) and of *S. cerevisiae* G_{1-59} (light green, PDB code 2 K88 [24]) and G_{61-101} (dark green) from yeast V-ATPase presented here, were aligned to a selection of homologous structures. The predicted assignments for $G_{102-114}$ of V-ATPase and H_{1-20} of A_1A_O ATP synthase are shown in grey colour. (B) Structure of *S. cerevisiae* G_{1-59} (light green) and G_{61-101} (dark green) from yeast V-ATPase superimposed on to the subunit H, H_{21-120}, of *T. thermophilus* (blue).

the other. The stretch of charged residue distributed on one side of the structure, attributed by Lys72, Lys 73, Glu75, Glu81, Glu84, Lys85, Lys86, Lys87 and Lys92 may be involved in its binding with the subunit A and B. This allows the hydrophobic residues like Ala64, Val67, Leu70, Ala74, Ala76, Val78, Leu82, Ala83, Ile85 and Ile88 to be part in the helix-helix interaction of subunit G and thereby a continuation of the hydrophobic stretch, described in the G_{1-59} solution structure [24]. The crosslink formation of the subunit G mutants demonstrate that the residues in position 72 and 72', 81 and 81' of the first and second helix are in close neighborhood as represented in the dimeric model of G_{61-101}, which is based on the crosslinking and docking data presented (Fig. 5C–D). In contrast, no crosslink product could be observed for the cysteine in position 74, reflecting the location of residue 74 at the opposite side of the two helices (Fig. 3B). A consequence of these results would be that the C-terminal helix of subunit G would not be arranged in a left-handed coiled-coil arrangement as proposed [41], since such fold is dictated by a heptad repeat $(a\text{-}b\text{-}c\text{-}d\text{-}e\text{-}f\text{-}g)_n$, with hydrophobic residues at positions *a* and *d* arranged at the interface between the two helices [45].

Most recently, the crystallographic structure of the related subunit H, including the residues 21 to 120, of the *Thermus thermophilus* A_1A_O ATP synthase was solved ([46], Fig. 6A). When positioned inside the crystallographic structure of H_{21-120} the two monomeric structures of G_{1-59} [24] as well as G_{61-101} accommodated very well, with r.m.s.d. values of 0.597 and 0.523 for G_{1-59} (residues Ser23–Ala40) and H_{21-120} (residues Ser25–Ala42) as well as G_{61-101} (residues Ala84–Val97) and H_{21-120} (residues Ser86–Val99), respectively (Fig. 6B). In addition, the structural model of the fitted NMR- and crystallographic structures of G_{1-59}, G_{61-101} and H_{21-120} reveals that the yeast V-ATPase subunit G forms a single α helix (excluding the residues 59–61, not defined so far), which appears to be a relatively inflexible structure. This is also in line with mutation studies in the N-terminal region, demonstrating that substitutions affect the enzyme in assembly and/or enzyme function [21]. However, deletions in the C-terminal end of subunit G from yeast did not alter the enzyme assembly or its function [21]. These data implied a more flexible, rope-like feature of the G subunit, giving this subunit the possible role of an elastic peripheral stalk for transient storage of energy between steps in the motion of the complex [46]. The available structures of the N- and C-terminal regions of the V-ATPase subunit G from yeast should now enable to generate appropriate mutant proteins and to measure the proposed elastic deformation of the stalk subunit G inside the enzyme complex by biophysical approaches.

Acknowledgements

S. Rishikesan is grateful to the authority of Nanyang Technological University (NTU) for awarding research scholarship. This research was supported by A*STAR BMRC (09/1/22/19/609). We thank Mr. Shovanlal Gayen (SBS, NTU) for helpful suggestions concerning NMR data analysis and art work.

Appendix A. Supplementary data

Supplementary data associated with this article can be found, in the online version, at doi:10.1016/j.bbamem.2010.06.012.

References

[1] K.W. Beyenbach, H. Wieczorek, The V-type H^+ ATPase: molecular structure and function, physiological roles and regulation, J. Exp. Biol. 209 (2006) 577–589.
[2] T. Nishi, M. Forgac, The vacuolar (H+)-ATPases-nature's most versatile proton pumps, Nature Mol. Cell Biol. 30 (2002) 94–103.
[3] J.S. Lolkema, Y. Chaban, E.J. Boekema, Subunit composition, structure, and distribution of bacterial V-Type ATPase, J. Bioenerg. Biomembr. 35 (2003) 323–336.
[4] S. Saroussi, N. Nelson, Vacuolar H^+-ATPase-an enzyme for all seasons, Pflugers Arch- Eur J. Physiol. 457 (2009) 581–587.
[5] G. Grüber, V. Marshanski, New insights into structure-function relationships between archeal ATP synthase(A_1A_O) and vacuolar type ATPase (V_1V_O), Bioessays 30 (2008) 1096–1099.
[6] M. Radermacher, T. Ruiz, H. Wieczorek, G. Grüber, Three-dimensional electron microscopy reveals the structure of the V_1-ATPase, J. Struct. Biol. 135 (2001) 26–37.
[7] V.F. Rizzo, Ü. Coskun, M. Radermacher, T. Ruiz, A. Armbrüster, G. Grüber, Resolution of the V_1-ATPase from *Manduca sexta* into subcomplexes and visualization of an ATPase active A_3B_3EG-complex by electron microscopy, J. Biol. Chem. 278 (2003) 270–275.
[8] J.P. Sumner, J.A.T. Dow, F.G. Earley, U. Klein, D. Jäger, H. Wieczorek, Regulation of plasma-membrane V-ATPase activity by dissociation of peripheral subunits, J. Biol. Chem. 270 (1995) 5649–5653.
[9] P. Dames, B. Zimmermann, R. Schmidt, J. Rein, M. Voss, B. Schewe, B. Walz, O. Baumann, cAMP regulates plasma membrane vacuolar-type H^+-ATPase assembly and activity in blowfly salivary glands, Proc. Natl. Acad. Sci. U.S.A. 103 (2006) 3926–3931.
[10] P.M. Kane, Disassembly and reassembly of the yeast vacuolar H^+-ATPase *in Vivo*, J. Biol. Chem. 270 (1995) 17025–17032.
[11] D.I. Svergun, S. Konrad, M. Huss, M.H.J. Koch, H. Wieczorek, K. Altendorf, V.V. Volkov, G. Grüber, Quaternary structure of V1 and F1 ATPase: significance of structural homologies and diversities, Biochemistry 37 (1998) 17659–17663.
[12] S. Wilkens, Z. Zhang, Y. Zheng, A structural model of the vacuolar ATPase from transmission electron microscopy, Micron 36 (2005) 109–126.
[13] K.C. Jefferies, M. Forgac, Subunit H of the V-ATPase inhibits ATP hydrolysis by the free V_1 domain by interaction with the rotary subunit F, J. Biol. Chem. 283 (2007) 4512–4519.
[14] T. Xu, E. Vasilyeva, M. Forgac, Subunit interactions in the clathrin-coated vesicle vacuolar (H^+)-ATPase complex, J. Biol. Chem. 274 (1999) 28909–28915.
[15] D. Venzke, I. Domgall, T. Kocher, J. Fethiere, S. Fischer, B. Böttcher, Elucidation of the stator organization in the V-ATPase of *Neurospora crassa*, J. Mol. Biol. 349 (2005) 659–669.
[16] A. Armbrüster, D.I. Svergun, Ü. Coskun, S. Juliano, S.M. Bailer, G. Grüber, Structural analysis of the stalk subunit Vma5p of the Yeast V-ATPase in solution, FEBS Lett. 570 (2004) 119–125.
[17] O. Drory, F. Frolow, N. Nelson, Crystal structure of yeast V-ATPase subunit C reveals its stator function, EMBO Rep. 5 (2004) 1148–1152.
[18] M. Sagermann, T.H. Stevens, B.W. Matthews, Crystal structure of the regulatory subunit H of the V-type ATPase of *Saccharomyces cerevisiae*, Proc. Natl. Acad. Sci. U.S.A. 98 (2001) 7134–7139.
[19] A. Armbrüster, S.M. Bailer, M.H.J. Koch, J. Godovac-Zimmermann, G. Grüber, Dimer formation of subunit G of the Yeast V-ATPase, FEBS Lett. 546 (2003) 395–400.
[20] A. Lipier, R. Gräf, M. Azuma, H. Merzendorfer, W.R. Harvey, H. Wieczorek, The peripheral complex of the Tobacco hornworm V-ATPase contains a novel 13-kDa subunit G, J. Biol. Chem. 271 (1996) 8502–8508.
[21] C.M.H. Charsky, N.J. Schumann, P.M. Kane, Mutational analysis of subunit G (Vma10p) of the yeast vacuolar H^+-ATPase, J. Biol. Chem. 275 (2000) 37232–37239.
[22] G.-H. Sun-Wada, Y. Imai-Senga, A. Yamamoto, Y. Murata, T. Hirata, Y. Wada, M. Futai, A proton pump ATPase with testis-specific E1-subunit isoform required for acrosome acidification, J. Biol. Chem. 277 (2002) 18098–18105.
[23] K. Hayashi, G.-H. Sun-Wada, Y. Wada, M. Nakanishi-Matsui, M. Futai, Defective assembly of a hybrid vacuolar H(+)-ATPase containing the mouse testis-specific E1 isoform and yeast subunits, Biochem. Biophys. Acta 1777 (2008) 1370–1377.
[24] S. Rishikesan, S. Gayen, R.Y. Thaker, S. Vivekanandan, M.S.S. Manimekalai, Y.H. Yau, S. Geifman Shochat, G. Grüber, Assembly of subunit d (Vma6p) and G (Vma10p) and the NMR solution structure of subunit G (G_{1-59}) of the *Saccharomyces cerevisiae* V_1V_O ATPase, Biochim. Biophys. Acta - Bioenerg. 1787 (2009) 242–251.
[25] G. Grüber, J. Godovac-Zimmermann, T.A. Link, Ü. Coskun, V.F. Rizzo, C. Betz, S. Bailer, Expression, purification and characterization of subunit E, an essential subunit of the vacuolar-ATPase, Biochem. Biophys. Res. Comm. 298 (2002) 383–391.
[26] U.K. Laemmli, Cleavage of structural proteins during the assembly of the head of bacteriophage T4, Nature 227 (1970) 680–685.
[27] D.G. Kneller, T.D. Goddard, SPARKY 3.105 edit, University of California, San Francisco, CA, 1997.
[28] M.V. Berjanskii, S. Neal, D.S. Wishart, PREDITOR: a web server for predicting protein torsion angle restraints, Nucleic Acids Res. 34 (2006) 63–69.
[29] K. Wüthrich, NMR of Proteins and Nuclei acids, Wiley, Interscience, New York, 1986.
[30] T. Herrmann, P. Güntert, K. Wüthrich, Protein NMR structure determination with automated NOE assignment using the new software CANDID and the torsion angle dynamics algorithm DYANA, J. Mol. Biol. 319 (2002) 209–227.
[31] R. Koradi, M. Billeter, K. Wüthrich, MOLMOL: a program for display and analysis of macromolecular structures, J. Mol. Graph. 14 (1996) 51–55.
[32] S.J. Gibbs, C.S.J. Johnson, A PFG NMR experiment for accurate diffusion and flow studies in the presence of eddy currents, J. Magn. Reson. 93 (1969) 395–402.
[33] D.K. Wilkins, S.B. Grimshaw, V. Receveur, C.M. Dobson, J.A. Jones, Hydrodynamic radii of native and denatured proteins measured by pulse field gradient NMR techniques, Biochemistry 38 (1999) 16424–16431.
[34] A. Tovchigrechko, I.A. Vakser, GRAMM-X public web server for protein-protein docking, Nucleic Acids Res. 34 (2006) 310–314.
[35] N. Guex, M.C. Peitsch, SWISS-MODEL and the Swiss-PdbViewer: an environment for comparative protein modeling, Electrophoresis 18 (1997) 2714–2723.
[36] K. Wüthrich, G. Wider, G. Wagner, W. Braun, Sequential resonance assignments as a basis for determination of spatial protein structures by high resolution proton nuclear magnetic resonance, J. Mol. Biol. 155 (1982) 311–319.

[37] S.K. Kandasamy, D.K. Lee, R.P.R. Naga, J. Xu, J.S. Santos, R.G. Larson, A. Ramamoorthy, Solid-state NMR and molecular dynamics simulations reveal the oligomeric ion-channels of TM2-GABAA stabilized by intermolecular hydrogen bonding, Biochem. Biophys. Acta 1778 (2009) 686–695.
[38] R.P.R. Naga, J.R. Brender, S. Vivekanandan, N. Popovych, A. Ramamoorthy, NMR structure in a membrance environment reveals putative amyloidogenic regions of the SEVI precursor peptide, J. Am. Chem. Soc. 131 (2009) 17972–17979.
[39] S. Rishikesan, Y.R. Thaker, R. Priya, S. Gayen, M.S.S. Manimekalai, C. Hunke, G. Grüber, Spectroscopic identification of residues of subunit G of the yeast V-ATPase in its connection with subunit E, Mol. Membr. Biol. 25 (2008) 400–410.
[40] R.P.O. Jones, L.J. Durose, J.B.C. Findlay, M.A. Harrison, Defined sites of interaction between subunit E (Vma4p), C (Vma5p), and G (Vma10p) within the stator structure of the vacuolar H^+-ATPase, Biochemistry 44 (2005) 3933–3941.
[41] N. Kitagawa, H. Mazon, A.J.R. Heck, S. Wilkens, Stoichiometry of the peripheral stalk subunits E and G of yeast V_1-ATPase determined by mass spectrometry, J. Biol. Chem. 283 (2008) 3329–3337.
[42] M. Lu, S. Vergara, L. Zhang, L.S. Holliday, J. Aris, S.L. Gluck, The amino-terminal domain of the E subunit of vacuolar H(+)-ATPase (V-ATPase) interacts with the H subunit and is required for V-ATPase function, J. Biol. Chem. 277 (2002) 38409–38415.
[43] M. Ohira, A.M. Smardon, C.M. Charsky, J. Liu, M. Tarsio, P.M. Kane, The E and G subunits of the yeast V-ATPase interacts tightly and are both present at more than one copy per V1 complex, J. Biol. Chem. 281 (2006) 22752–22760.
[44] I.E. Hunt, B.J. Bowman, The Intriguing evolution of the "b" and "G" Subunit in F-type and V-type ATPase: Isolation of the *vma*-10 gene from *Neurospora crassa*, J. Bioenerg. Biomembr. 29 (1997) 533–540.
[45] D.A. Parry, R.D. Fraser, J.M. Squire, Fifty years of coiled-coils and α-helical bundles: a close relationship between sequence and structure, J. Struct. Biol. 163 (2008) 258–269.
[46] L.K. Lee, A.G. Stewart, M. Donohoe, R.A. Bernal, D. Stock, The structure of the peripheral stalk of *Thermus thermophilus* H^+-ATPase/synthase, Nat. Struct. Mol. Biol. 17 (2010) 373–378.
[47] W.L. DeLano, The pyMol Molecular Graphics System San Carlos, CA: DeLano Scientific, 2001.